processes

Article

The Synergistic Effect of CeO_2 and Micron-Cu Enhances the Hydrogenation of CO_2 to CO

Bowen Lu [1,†], Huiying Sang [1,†], Liang Liu [2], Zhijian Yu [3], Yaqin Guo [4] and Yongqing Xu [1,3,*]

1 State Key Laboratory of Coal Combustion, School of Energy and Power Engineering, Huazhong University of Science and Technology, Wuhan 430074, China
2 Key Laboratory of New Materials and Facilities for Rural Renewable Energy of Ministry of Agriculture and Rural Affairs, College of Mechanical & Electrical Engineering, Henan Agricultural University, Zhengzhou 450002, China
3 Key Laboratory for Thermal Science and Power Engineering of Ministry of Education, Beijing Key Laboratory of CO_2 Utilization and Reduction Technology, Department of Energy and Power Engineering, Tsinghua University, Beijing 100084, China
4 Ministry of Education Key Laboratory for Earth System Modeling, Department of Earth System Science, Tsinghua University, Beijing 100084, China; yaqin_guo@mails.tsinghua.edu.cn
* Correspondence: xuyongqing@hust.edu.cn
† These authors contributed equally to this work.

Abstract: The catalytic applications of micron Cu powder are limited due to its large particle size and small specific surface area. Modifying micro-Cu powder to achieve a high catalytic performance is a challenge in the application of micron copper. In this work, micro-Cu was used to synthesize a CeO_2–Cu catalyst, and the phase composition and surface pore structure were analyzed using XRD, BET, etc. The CO_2 hydrogenation performance of the CeO_2–Cu catalyst was analyzed in comparison with CeO_2 and Cu, and we found that the CeO_2–Cu catalyst exhibited a synergistic effect between Cu and cerium, resulting in a much higher hydrogenation performance at 500 °C than CeO_2 or Cu alone. H_2-TPR and TEM characterization revealed that the CeO_2–Cu catalyst formed interfacial interactions with a relatively large Ce–Cu interface, where cerium oxide could promote the reduction of CuO and lower the reduction temperature. Additionally, cerium oxide formed a confinement structure for Cu, and the CeO_2–Cu catalyst exhibited a higher oxygen vacancy concentration, thereby promoting the CO_2 hydrogenation performance. Cu–CeO_2 interaction provides valuable insights into the catalytic application of micron Cu powder.

Keywords: RWGS reaction; Cu–CeO_2 interface; micro-Cu; synergistic effect; oxygen vacancy

check for updates

Citation: Lu, B.; Sang, H.; Liu, L.; Yu, Z.; Guo, Y.; Xu, Y. The Synergistic Effect of CeO_2 and Micron-Cu Enhances the Hydrogenation of CO_2 to CO. *Processes* **2024**, *12*, 1912. https://doi.org/10.3390/pr12091912

Academic Editor: Adina Musuc

Received: 29 July 2024
Revised: 24 August 2024
Accepted: 3 September 2024
Published: 6 September 2024

1. Introduction

As industrialization accelerates, the demand for energy from humans is increasing, leading to the consumption of a large amount of fossil energy and the emission of a large amount of CO_2 into the atmosphere, disrupting the atmospheric carbon balance [1,2]. The increase in CO_2 concentration triggers a series of environmental problems, such as ocean acidification and the greenhouse effect [3–6]. The rising global temperature not only accelerates the melting of the Arctic glaciers and the rise in sea levels but also increases the frequency of extreme weather events, causing damage to the human living environment [7]. Therefore, reducing CO_2 emissions and in doing so lowering the concentration of CO_2 in the atmosphere is an urgent challenge that needs to be addressed [8–10].

The hydrogenation of CO_2 is currently one of the most researched and effective methods for CO_2 reduction [9,11,12]. This involves using unstable electricity generated from renewable energy sources (such as solar and wind power) to electrolyze water for hydrogen production, and then obtaining high-value-added products such as CO, methane, and ethylene through the hydrogenation of CO_2 [13–16]. CO_2 hydrogenation reduces the concentration of carbon dioxide in the atmosphere and converts CO_2 into high-value-added products, generating economic benefits [17]. Among various CO_2 hydrogenation methods, the process of converting CO_2 to CO via an RWGS reaction is widely studied due to the high application flexibility of the resulting CO [18]. CO, as the main component of syngas, can be utilized not only for methanol synthesis but also for the Fischer–Tropsch (F-T) reaction [19–21]. Additionally, CO can be applied in chemical reactions to synthesize acetic acid, phosgene, and other substances [18]. Due to the endothermic nature of the reverse water–gas shift (RWGS) reaction under atmospheric pressure, the reaction requires high temperatures [22]. However, high temperatures can lead to catalyst deactivation and hydrogenation side reactions, resulting in reduced CO selectivity [23]. Therefore, it is necessary to design efficient catalysts to lower the reaction temperature and regulate product selectivity.

Cu-based catalysts have been widely applied in CO_2 hydrogenation reactions in recent years due to their low reduction temperature and excellent hydrogenation CO selectivity [24]. However, the CO_2 hydrogenation conversion activity in the low-temperature conditions is relatively low [25–27]. Chen's research revealed that the RWGS reaction mainly occurs at the metal–support interface, where the metal activates the hydrogen molecule and the metal–support interface adsorbs and activates CO_2 [11,28]. Increasing the metal–support interface will thus be beneficial for the RWGS reaction [29,30]. Currently, catalyst design research has primarily focused on nano-Cu catalysts, while micron-sized Cu powder produced from ball milling of industrial waste copper has received less application due to its large particle size and small specific surface area, resulting in poor CO_2 hydrogenation activity [31]. Therefore, modifying the micron-sized Cu powder to improve its catalytic capability presents a current challenge in applying industrial waste copper in CO_2 catalytic reactions.

The interfacial structure of the metal and oxide support plays a pivotal role in the reverse water–gas shift (RWGS), and reconstructing the Cu–CeO_2 interface will improve CO_2 hydrogenation performance [30,32,33]. Zhang and co-workers found that the Cu–CeO_2 interface is related to the RWGS activity, and increasing the Cu–CeO_2 interface benefits CO generation [24]. Furthermore, Zhou et al. found that Cu can be doped into the CeO_2 lattice, increasing CeO_2 lattice spacing, resulting in more Ce^{3+} formation, and inducing the generation of more oxygen vacancies, and that the oxygen vacancies together with Ce^{3+} can serve as active sites to activate CO_2 and enhance the CO_2 hydrogenation reaction [34]. Our previous work also demonstrated that Cu interacted with CeO_2 to form a Cu–O–Ce interface and induced more oxygen vacancy formation [31]. The oxygen vacancies around the Cu–CeO_2 interface enhanced CO_2 adsorption and promoted CO_2 conversion. CO_2 reacted with active hydrogen to form COOH, and then COOH species dissociated into CO and OH adsorbed on the surface of Cu–CeO_2. Therefore, constructing a Cu–CeO_2 interface may be advantageous for enhancing micro-Cu CO_2 hydrogenation performance. However, little work has investigated the relationship between Cu and CeO_2, though it may play a vital role in understanding the CO_2 hydrogenation performance of Cu–Ce-based catalysts.

In this work, the CeO_2–Cu catalyst was synthesized with micron-sized Cu, and the ceria–Cu interface was constructed for CO_2 utilization. The phase composition and surface pore structure information of the CeO_2–Cu catalyst were analyzed with XRD, BET, etc. The catalytic performance of CO_2 hydrogenation was analyzed and compared with CeO_2 and Cu alone. A synergistic effect appeared with Cu and cerium oxide. H_2-TPR and TEM characterization were measured to reveal the CeO_2–Cu interfacial interactions and CeO_2 effect on micro-Cu. Additionally, the CeO_2–Cu structure and oxygen vacancy information were investigated to reveal the enhancement of CeO_2 for CO_2 hydrogenation performance.

2. Experimental Section

2.1. Synthesis of Catalysts

All the chemicals (micro Cu, $Ce(NO_3)_3 \cdot 6H_2O$) were purchased from Aladdin Chemistry Co., Ltd., Shanghai, China without any further purification. The CeO_2–Cu catalyst was synthesized using a precipitation method. Firstly, a certain amount of $Ce(NO_3)_3{\cdot}6H_2O$ was dispersed and dissolved in ethanol, and then 0.5 g of micro-Cu powder was added, followed by stirring at room temperature for 30 min. Subsequently, a grey solid was obtained by adding ammonia water for precipitation, which was washed three times with water by centrifugation, and then dried to obtain the grey–black sample named CeO_2–Cu. The CeO_2 catalyst was also synthesized using a precipitation method. Initially, a certain amount of $Ce(NO_3)_3{\cdot}6H_2O$ was dispersed and dissolved in water, and then a grey solid was obtained by adding ammonia water for precipitation; the solid was washed three times with water by centrifugation, and then dried to obtain the light yellow sample named CeO_2.

2.2. Characterization

X-ray powder diffraction (XRD) was employed using a D8 X-ray diffractometer (from Bruker AXS, Karlsruhe, Germany) to conduct crystal structure analysis of CeO_2–Cu, CeO_2, and Cu samples. Cu K_α (λ = 0.15418 nm) was utilized with parameters set at 40 kV, 40 mA, a testing range from 20 to 80°, and a scan step size of 0.01313°. The final spectrum was compared with the JCPDS card library to determine the composition of the powders. The BET surface area analyzer 3H-2000PS (Beishide Instrument Technology (Beijing) Co., Ltd., Beijing, China) was used to investigate differences in pore size distribution and specific surface area of the CeO_2–Cu, CeO_2, and Cu samples. Before the BET testing, all the materials were pre-heated at 180 °C for 180 min to decrease the absorbed gases. The scanning transmission electron microscope (STEM) Talos F200X (from FEI, Eindhoven, The Netherlands) was utilized to analyze the elemental composition of the CeO_2–Cu, CeO_2, and Cu samples, as well as to select a line for energy-dispersive X-ray spectroscopy (EDS) analysis. Prior to the TEM analysis, the CeO_2–Cu, CeO_2, and Cu samples were pretreated under ultra-sonication for 0.5 h, to achieve a uniform dispersion in an ethanol solvent, and then with the evaporation of three suspensions dropped on a gold grid.

Hydrogen Temperature Programmed Reduction (H_2-TPR) was performed using a chemisorption analyzer (AutoChem II, Micromeritics, Norcross, GA, USA), and the hydrogen signal was monitored and analyzed online using a TCD detector. CeO_2–Cu, CeO_2, and Cu samples were first pretreated at 400 °C with pure He gas (30 mL/min) for 20 min to degas the adsorbed molecules (such as oxygen, nitrogen, carbon dioxide, or water), and then cooled to room temperature before introducing 10% H_2/Ar (30 mL/min). Subsequently, the samples underwent programmed temperature ramping from 30 °C to 500 °C at a rate of 10 °C/min. The H_2 consumption during the temperature ramping was determined with a TCD detector. LabRAM HR800 (LabRAM Odyssey, Longjumeau, France) was measured to collect Raman spectroscopy of the CeO_2–Cu, CeO_2, and Cu samples.

2.3. Evaluation of Catalytic Performance

The performance of CeO_2–Cu, CeO_2, and Cu catalysts was evaluated with a microreactor furnace (PH950, Apera Instruments, Shanghai, China) under atmospheric pressure. First, 50 mg of the catalyst was loaded into a U-shaped tube (d = 8 mm) and subjected to a pre-reduction treatment at 400 °C in a reducing atmosphere. After cooling to room temperature, the reactants (1%CO_2 + 4%H_2 + 95%Ar, Ar was balanced gas) were introduced, and the temperature was ramped up at a rate of 10 °C/min for activity testing in the range of 500−700 °C. Online analysis of CO_2 hydrogenation products was performed using gas chromatography (GC-2020, Hengxin, Jiangsu, China), which was equipped with packed columns (ZKAT-Z13 PLOT, ATEO) and a flame ionization detector with mechanized nickel, which exhibited the separation and quantification of CO_2, CO, and CH_4. The formula for calculating the CO_2 conversion rate and CO selectivity are listed as follows:

$$CO_2\ \text{Conversion} = ([CO_2]_{in} - [CO_2]_{out})/[CO_2]_{int} * 100\%$$

$$CO\ \text{Selectivity} = [CO]_{out}/([CO_2]_{in} - [CO_2]_{out}) * 100\%$$

3. Results and Discussion

3.1. Characterization

In order to study the effect of cerium addition on the structure of micro-copper powders, XRD characterization was performed on CeO_2–Cu, CeO_2, and micro-Cu, and the results are shown in Figure 1. The peaks located at 28.549°, 33.077°, 47.483°, 56.342°, 59.09°, 69.416°, 76.704°, and 79.077° could be assigned to the fluorite cubic structure of CeO_2 (JCPDS#34-0394). The peaks located at 43°, 51°, and 74° were consistent with the Cu metallic phase (CPDS#04-0836). It can be observed that in the XRD spectrum of the CeO_2–Cu sample synthesized with cerium nitrate, the signal for CeO_2 is weak, the peak for Cu is strong, and there is essentially no peak for CuO. Micro-Cu exhibited a strong Cu peak, while the signal intensity for the cerium oxide sample was relatively weak, consistent with the weak CeO_2 signal for the CeO_2–Cu sample, indicating poor crystallinity of CeO_2 prepared by the cerium nitrate precipitation method. The weak signal peak for CeO_2 in CeO_2–Cu may be attributed to the strong interaction between Ce and Cu. The Cu signal peaks in the CeO_2–Cu synthesized from the cerium nitrate precursor and in the micro-Cu both exhibited strong signals, with the Cu signal peak in micro-Cu was stronger than that in CeO_2–Cu, indicating a possible interaction between cerium oxide and Cu, leading to a weakening of the metal Cu signal peak. The difference in the signal peaks of Cu substances suggests an interaction between CeO_2 and micrometer-sized Cu. The interaction between CeO_2 and micrometer-sized Cu may lead to the formation of more oxygen vacancies in CeO_2, which could potentially promote reactivity.

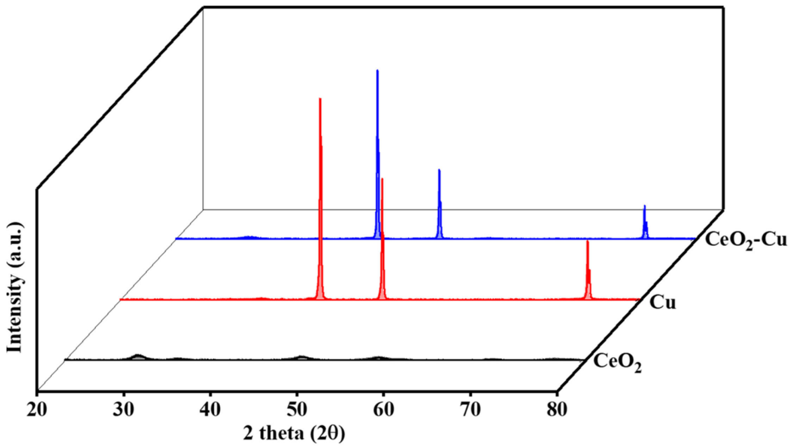

Figure 1. XRD patterns for CeO_2–Cu, CeO_2, and micro-Cu.

To study the effect of cerium addition on the surface pore structure of micro-Cu powder, a specific surface area analysis was conducted on CeO_2–Cu, CeO_2, and micro-Cu. The results of nitrogen adsorption–desorption isotherms and pore size distribution are shown in Figure 2, while the specific surface area and average pore size results are presented in Table 1. After loading with ceria species, the specific surface area of CeO_2–Cu was larger than that of micro-Cu but smaller than that of ceria, and the pore size distribution shifted towards that of CeO_2. There was a significant difference in the pore size distribution between CeO_2–Cu and micro-Cu, indicating that ceria addition has an impact on the pore size distribution of Cu and that the difference in the pore size distribution of CeO_2–Cu may result from the interaction between CeO_2 and micro-Cu.

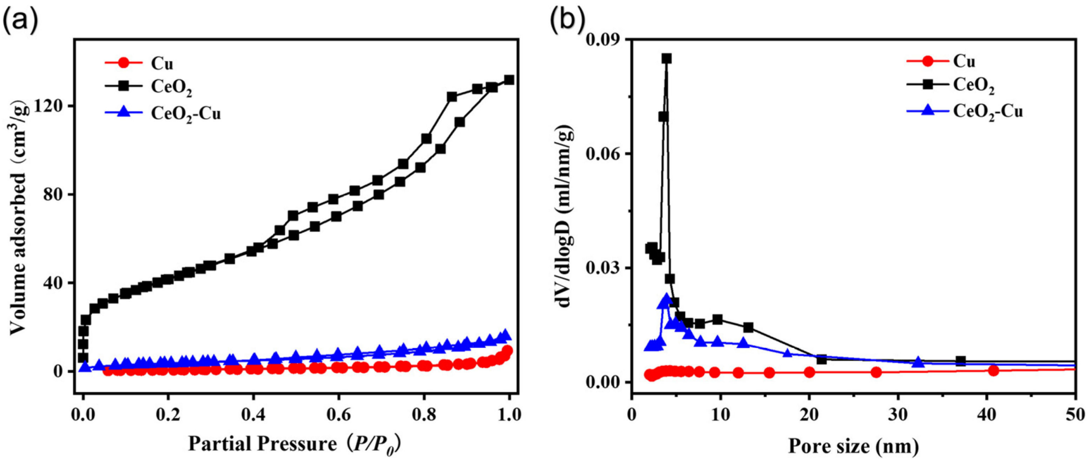

Figure 2. (**a**). N_2 adsorption–desorption isotherms and (**b**) pore diameter distributions of CeO_2–Cu, CeO_2, and Cu catalysts.

Table 1. Specific surface areas and pore information of CeO_2–Cu, CeO_2, and Cu catalysts.

Catalyst	g_{CeO2}/g_{Cu} (Wt%)	S_{BET} (m^2/g)	Pore Volume (mL/g)	Average Pore Diameter (nm)
Cu		2.68	0.22	12.36
CeO_2		149.87	0.407	5.02
CeO_2–Cu	20	13.54	0.0277	6.03

3.2. CO_2 Hydrogenation Performance

To analyze the effect of cerium addition on the catalytic performance of micro-Cu, the CO_2 hydrogenation activities of CeO_2–Cu, CeO_2, and Cu micro-powders were studied. Activity tests were conducted in the 500−700 °C range, and the CO_2 hydrogenation activities of CeO_2–Cu, CeO_2, and Cu catalysts are shown in Figure 3. At 500 °C, the CO_2 hydrogenation activity of the CeO_2–Cu catalyst reached 49.82%, which is more than 204 times higher than that of the Cu catalyst (0.244%). In contrast, the CeO_2 catalyst showed minimal CO_2 hydrogenation activity at this temperature (4.627%), and the CO selectivity of all three catalysts for CO_2 hydrogenation was 100%. The results of CO_2 hydrogenation activities for CeO_2–Cu, CeO_2, and Cu catalysts indicated a synergistic effect between Cu and CeO_2 in CeO_2–Cu. While the CO_2 conversion activity of individual Cu or CeO_2 was poor at 500 °C, when Cu was combined with ceria, Cu–CeO_2 supported more active sites for the RWGS reaction, exhibiting a higher CO_2 conversion rate. These results suggested that both ceria and copper are involved in the CO_2 hydrogenation process, with Cu playing a key role in activating hydrogen at moderate temperatures, while ceria provides active sites to promote CO_2 activation and form carbonates for further hydrogenation conversion [11,24].

Increasing the temperature can promote the activation of CO_2 and H_2 molecules, thereby enhancing the CO_2 hydrogenation activity. At high temperatures, the CO selectivity of the CO_2 hydrogenation products for CeO_2–Cu, CeO_2, and Cu catalysts is 100%, indicating that the ceria addition does not affect the hydrogenation selectivity of Cu under atmospheric pressure conditions. These results were consistent with the results of previous studies on Cu-catalyzed hydrogenation [31,35]. Under atmospheric pressure, CuO species were reduced to a metallic state and exhibited high CO selectivity during the CO_2 hydrogenation process.

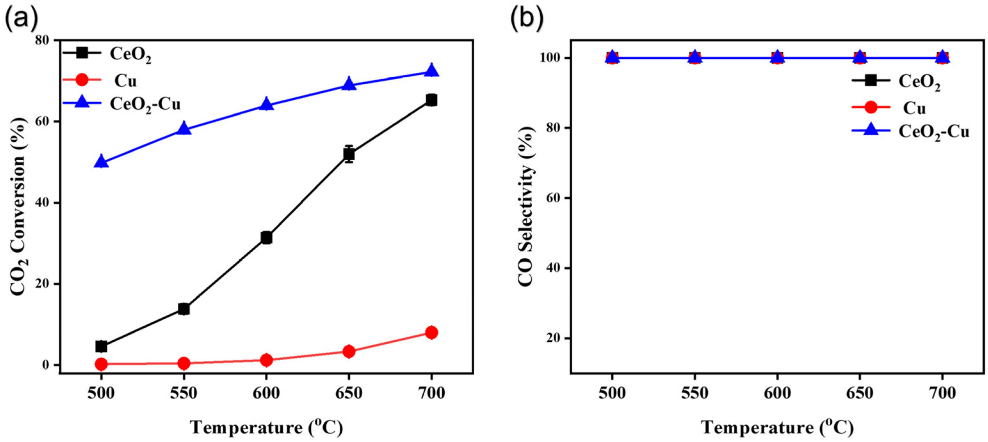

Figure 3. Hydrogenation performance of CeO_2–Cu, CeO_2, and Cu: (**a**) CO_2 conversion activity, (**b**) CO selectivity (100 mL/min).

The hydrogenation performance of the cerium oxide was reported to be mainly determined by oxygen vacancies on the CeO_2 surface, and oxygen vacancies were key to activating hydrogen molecules [36]. Pure cerium oxide exhibited relatively poor activity, and increasing the temperature could significantly promote the hydrogenation activity of cerium oxide. In the Cu–CeO_2 catalyst system, the metal Cu can activate hydrogen molecules at low temperatures, producing active hydrogen, which then interacts with activated carbonates to produce formate or carboxylate and further hydrogenates to generate CO and water. During the RWGS reaction, the CO_2 conversion activity of Cu–CeO_2 at 500 °C is nearly 10.7 times higher than that of cerium oxide, possibly due to the reduction properties of the metal Cu, and the active Cu sites are beneficial for hydrogen activation. At 700 °C, the CO_2 hydrogenation activity of CeO_2–Cu is similar to that of CeO_2 catalysts, and it was 8.9 times higher than that of micro-Cu. Increasing the temperature induced a similar hydrogenation behavior between Cu–CeO_2 and cerium oxide, indicating that Cu metal has little effect on hydrogenation activity. CeO_2 could provide a function of H_2 activation and CO_2 activation, and the CO_2 conversion rate was no longer limited by hydrogen activation at high temperatures. Previous studies revealed that hydrogen activation is no longer the main limitation of cerium oxide under high-temperature conditions; instead, the activation of CO_2 molecules becomes the main factor affecting its activity [36–38]. Therefore, the micro-Cu catalyst exhibited relatively poor hydrogenation activity at 700 °C. On the surface of Cu, the surface charge is not conducive to the activation of CO_2 molecules, hence the poor catalytic activity of Cu [39]. The construction of Cu–CeO_2 can induce Cu–CeO_2 interface formation, thereby significantly enhancing the CO_2 hydrogenation activity via the interface oxygen vacancies and achieving efficient CO_2 conversion [40]. Metal Cu and oxygen vacancies around the Cu–CeO_2 interfacial area could serve as active sites for the RWGS reaction. Therefore, a higher CO_2 conversion rate appeared for Cu–CeO_2 than Cu or CeO_2 solely, and there was a synergistic effect between Cu and cerium oxide with Cu–CeO_2, enhancing the RWGS reaction performance.

3.3. CeO_2 Effect on Micro-Cu

In order to study the influence of CeO_2 addition on the microstructure of micro-Cu, the morphologies of CeO_2–Cu, CeO_2, and Cu were characterized, and the results obtained from transmission electron microscopy (TEM) are shown in Figure 4. The micro-Cu particles exhibited spherical shapes with relatively large sizes, with an average particle size distribution of 1.88 μm (Cu powders were dispersed in water, and the size distribution of micron Cu powders was measured using a mastersizer 2000, Malvern Instruments, Malvern, UK), and there could be some CuO_x species on the surface of micron Cu (Figure 4a) [31].

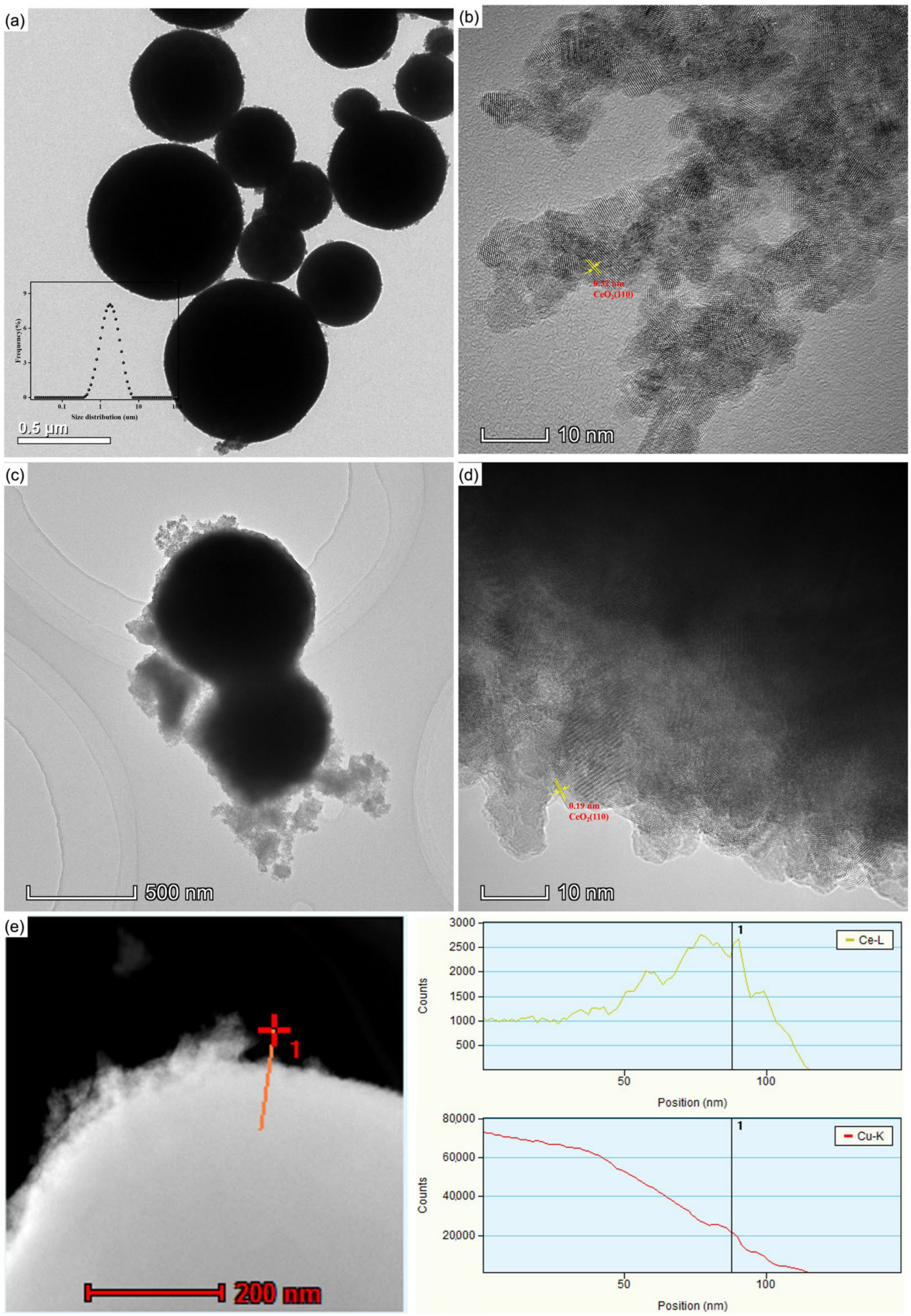

Figure 4. TEM images of CeO_2–Cu, Cu, and CeO_2: (**a**) TEM image of Cu powder, (**b**) HRTEM of CeO_2, (**c**) TEM image of CeO_2–Cu powder, (**d**) HRTEM of CeO_2–Cu, (**e**) HADDF of CeO_2–Cu, and line distribution of Ce and Cu.

CeO_2 prepared by ammonia precipitation displayed relatively small particles, mainly showing the (110)-crystal facet (Figure 4b). The CeO_2–Cu catalyst mainly presents a morphology where CeO_2 wraps around micron Cu, while some cerium oxide is in a dispersed state. The synthesized CeO_2–Cu appeared similar in morphology to the micron Cu material. In Figure 4c, the black area within the large spherical particles represents the metal Cu particles, while the surrounding white shadows indicate the presence of cerium oxide. Micro-Cu was confined with CeO_2 species, and the CeO_2 shell was relatively thin. To further reveal information on the CeO_2–Cu interface, TEM energy-dispersive X-ray spectroscopy (EDS) was used to investigate the elemental distribution on the surface of

CeO_2–Cu. It was found that the edge of the spherical CeO_2–Cu is mainly composed of cerium oxide. Figure 4d,e illustrate that the cerium oxide distribution is relatively uniform, with CeO_2 being the main component on the surface of the catalyst. When the Ce peak reaches its maximum, there is a localized increase in the Cu signal peak, indicating a higher local content of Cu elements in the cerium oxide region, possibly due to the interaction between CeO_2 and Cu.

CeO_2 addition on the surface of micro-Cu resulted in CeO_2–Cu interactions, which impacted the microstructural porosity and surface elemental distribution of Cu. In order to understand the influence of cerium oxide addition on the reduction performance of Cu catalysts, H_2-TPR tests were conducted on CeO_2–Cu, Cu, and CeO_2 catalysts, as shown in Figure 5. The reduction peak of micrometer-sized Cu appeared at 276 °C, mainly stemming from the reduction peak of the surface copper oxide on micrometer-sized Cu [31]. The reduction peak of cerium oxide appeared at 460 °C, primarily originating from the reduction peak of the oxygen adsorbed on the surface of cerium oxide [24]. For CeO_2–Cu, two reduction peaks were observed between 100 and 300 °C, attributed to the reduction peaks of Cu_2O and CuO_x, which strongly interact with CeO_2. The addition of cerium oxide led to a shift in the reduction peak position of Cu, indicating that the addition of cerium oxide facilitated the reduction of CuO, consistent with the conclusion that CeO_2 promotes the reduction of CuO_x in the Cu–Ce system [11].

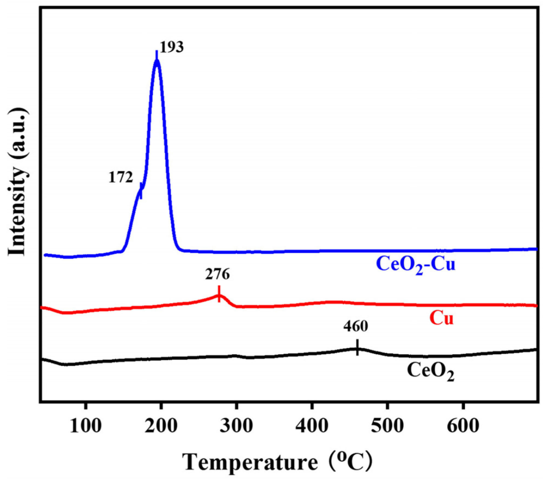

Figure 5. H_2-TPR of CeO_2–Cu, Cu, and CeO_2 catalysts.

In order to further analyze the enhancement effect of CeO_2 addition on Cu, Raman spectroscopy was conducted to confirm the role of oxygen vacancies of CeO_2–Cu and CeO_2 catalysts, and the results are shown in Figure 6. Two peaks appeared in the region of 200−800 cm^{-1}. The strong peak that appeared at 456 cm^{-1} could correspond to the F_{2g} vibration mode of local octahedral symmetry in CeO_2. The broad Raman peak that appeared at around 600 cm^{-1} could be ascribed to the lattice-defect-induced (D) mode resulting from oxygen defects. The presence of oxide peaks on the surface of micron Cu indicated the existence of CuO_x species [41]. After adding cerium oxide to micro-Cu, the F_{2g} vibration peak of cerium oxide significantly weakened, possibly due to the interaction between Cu and CeO_2. A reduction in the F_{2g} peak and a low Raman shift to the D peak appeared on CeO_2–Cu, indicating the presence of a Cu–O–CeO_2 structure [40]. The value of I_D/I_{F2g} was calculated to reveal the concentration of oxygen vacancies in the CeO_2–Cu and CeO_2 catalysts. It was found that the oxygen vacancy concentration (I_D/I_{F2g} = 0.387) on the surface of CeO_2–Cu was higher than that of pure CeO_2 (I_D/I_{F2g} = 0.062). The oxygen vacancy concentration was regarded as the leading active site for the CO_2 hydrogenation reaction, capable of activating CO_2 molecules to produce carbonates for further hydrogenation to produce CO [36,42]. Therefore, Cu–CeO_2 exhibited higher hydrogenation activity than that of cerium oxide at 700 °C during the hydrogenation process.

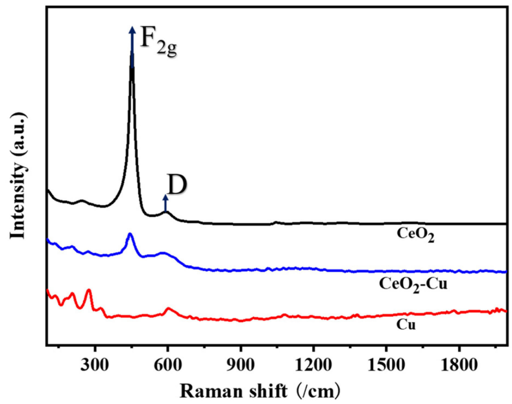

Figure 6. Raman spectrum of CeO_2–Cu, Cu, and CeO_2 catalysts.

Metal sintering at high temperatures under a reduced atmosphere was the leading cause of deactivation during the RWGS reaction. A long-lifetime reaction test is a crucial indicator to evaluate the CeO_2–Cu catalyst. The stability test of the RWGS reaction was operated at 700 °C, and it was found that the CeO_2–Cu catalyst maintained good stability (Figure 7). The microstructure of Cu–CeO_2 after the RWGS reaction was analyzed to reveal the elemental distribution of Cu–CeO_2. It was observed that after high-temperature reactions, cerium oxide particles underwent sintering and increased in size, while micro-Cu was enveloped by a shell formed by cerium oxide (Figure 8). Therefore, Cu–CeO_2 exhibits good CO_2 hydrogenation stability at high temperatures.

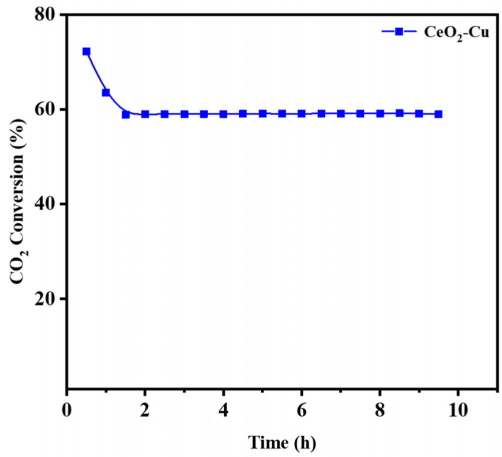

Figure 7. CO_2 conversion of the CeO_2–Cu catalyst at 700 °C and a flow speed of 100 mL/min.

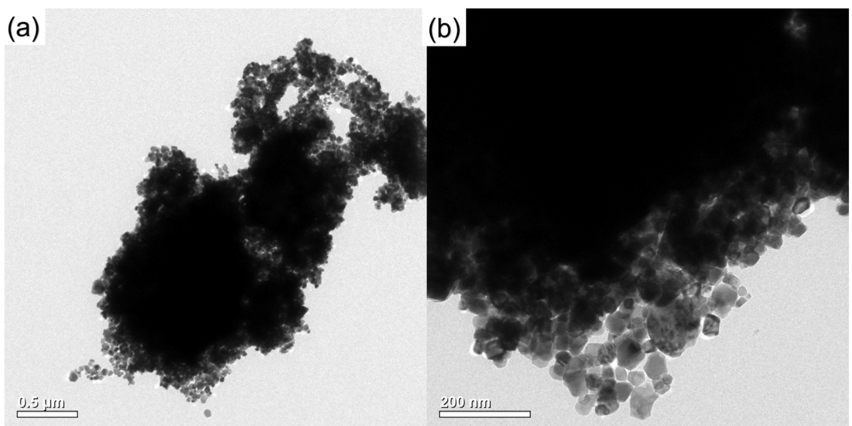

Figure 8. TEM image (**a**) and HRTEM image (**b**) of CeO_2–Cu after RWGS reaction.

4. Conclusions

This work focused on the synthesis of a CeO_2–Cu catalyst, by introducing cerium salt on the surface of micron Cu, and applied the RWGS reaction. The experimental results indicated that the modified CeO_2–Cu catalyst demonstrated efficient activity in the CO_2 hydrogenation process. Specifically, CeO_2–Cu exhibited a superior catalytic performance, reaching a conversion rate of 49.82% at 500 °C, which was 204 times higher than that of micro-Cu and 10.9 times higher than that of CeO_2. A synergistic effect appeared between CeO_2 and Cu species within the CeO_2–Cu catalyst. Cu species and oxygen vacancies formed around the Cu–CeO_2 interface, which enhanced the CO_2 hydrogenation performance. Furthermore, results from TEM and BET analysis confirmed the CeO_2-confined structure in the CeO_2–Cu catalyst, as well as the existence of a significant Ce–Cu interface. These structural characteristics contribute to the catalyst's excellent CO_2 hydrogenation performance.

Micron-sized Cu powders are generated through ball-milling from industrial waste copper. The application of micron Cu is usually limited due to its large particle size and small specific surface area. Modified micro-Cu powder, designed to overcome this limitation and achieve a high catalytic performance, offers an insight into the application potential of industrial waste copper.

Author Contributions: B.L.: methodology, formal analysis, writing—original draft, writing—review and editing. H.S.: formal analysis, writing—original draft. L.L.: resources, formal analysis, writing—original draft. Z.Y.: formal analysis, writing—original draft. Y.G.: writing—review and editing, visualization. Y.X.: writing—review and editing, resources, funding acquisition. All authors have read and agreed to the published version of the manuscript.

Funding: This research was funded by the National Natural Science Foundation of China (52206147) and the China Postdoctoral Science Foundation (grant 2023M741884).

Data Availability Statement: The data presented in this study are available on request from the corresponding author.

Acknowledgments: This research was funded by the National Natural Science Foundation of China (52206147) and the China Postdoctoral Science Foundation (grant 2023M741884). The authors are also thankful for Zhongkebaice Technology Service Co., Ltd. (Beijing, China) providing training on and access to measurements for the TEM, H_2-TPR, Raman, and XRD testing.

Conflicts of Interest: The authors declare no conflict of interest.

References

1. Chen, J.; Xu, Y.; Liao, P.; Wang, H.; Zhou, H. Recent progress in integrated CO_2 capture and conversion process using dual function materials: A state-of-the-art review. *Carbon Capt. Sci. Technol.* **2022**, *4*, 100052. [CrossRef]
2. Ma, J.; Kong, H.; Wang, J.; Zhong, H.; Li, B.; Song, J.; Kammen, D.M. Carbon-neutral pathway to mitigating transport-power grid cross-sector effects. *Innovation* **2024**, *5*, 100611. [CrossRef] [PubMed]
3. Mathias Dautzenberg, F.; Lu, Y.; Xu, B. Controlling the global mean temperature by decarbonization. *Acta Phys.-Chim. Sin.* **2020**, *37*, 2008066. [CrossRef]
4. Dai, A.; Luo, D.; Song, M.; Liu, J. Arctic amplification is caused by sea-ice loss under increasing CO_2. *Nat. Commun.* **2019**, *10*, 121. [CrossRef] [PubMed]
5. Scanes, E.; Scanes, P.R.; Ross, P.M. Climate change rapidly warms and acidifies Australian estuaries. *Nat. Commun.* **2020**, *11*, 1803. [CrossRef]
6. Geng, T.; Jia, F.; Cai, W.; Wu, L.; Gan, B.; Jing, Z.; Li, S.; McPhaden, M.J. Increased occurrences of consecutive la niña events under global warming. *Nature* **2023**, *619*, 774–781. [CrossRef]
7. Zantye, M.S.; Arora, A.; Hasan, M.M.F. Renewable-integrated flexible carbon capture: A synergistic path forward to clean energy future. *Energy Environ. Sci.* **2021**, *14*, 3986–4008. [CrossRef]
8. Hepburn, C.; Adlen, E.; Beddington, J.; Carter, E.A.; Fuss, S.; Mac Dowell, N.; Minx, J.C.; Smith, P.; Williams, C.K. The technological and economic prospects for CO_2 utilization and removal. *Nature* **2019**, *575*, 87–97. [CrossRef]
9. Shi, Y.; Shou, H.; Li, H.; Zhan, G.; Liu, X.; Yang, Z.; Mao, C.; Cheng, J.; Zhang, X.; Jiang, Y.; et al. Visible light-driven conversion of carbon-sequestrated seawater into stoichiometric co and HClO with nitrogen-doped BiOCl atomic layers. *Angew. Chem. Int. Ed.* **2023**, *62*, e202302286. [CrossRef]

10. Jing, R.; Wang, R.; Xing, L.; Li, Q.; Wang, L. Industrial perspective on the current status of carbon capture application in china's nonpower industries. *Sep. Purif. Technol.* **2024**, *334*, 125993. [CrossRef]
11. Porosoff, M.D.; Yan, B.; Chen, J.G. Catalytic reduction of CO_2 by H_2 for synthesis of CO, methanol and hydrocarbons: Challenges and opportunities. *Energy Environ. Sci.* **2016**, *9*, 62–73. [CrossRef]
12. Kattel, S.; Liu, P.; Chen, J.G. Tuning selectivity of CO_2 hydrogenation reactions at the metal/oxide interface. *J. Am. Chem. Soc.* **2017**, *139*, 9739–9754. [CrossRef] [PubMed]
13. Wang, Y.; Winter, L.R.; Chen, J.G.; Yan, B. CO_2 hydrogenation over heterogeneous catalysts at atmospheric pressure: From electronic properties to product selectivity. *Green Chem.* **2021**, *23*, 249–267. [CrossRef]
14. Wang, I.; Huang, S.; Wang, S.; Bie, X.; Zhou, H.; Li, Z. Mechanistic study of integrated CO_2 capture and utilization over cu and al-modified calcined limestone with high stability using mfb-tga-ms. *Sep. Purif. Technol.* **2024**, *333*, 125975. [CrossRef]
15. Fatimah, M.; Qyyum, M.A.; Lee, M.; Alshareef, R.S.; Aslam, M.; Saeed, B.; Dai, L.; Gilani, M.A.; Bazmi, A.A.; Chang, I.S.; et al. Industrial waste gases as a resource for sustainable hydrogen production: Resource availability, production potential, challenges, and prospects. *Carbon Capt. Sci. Technol.* **2024**, *12*, 100228. [CrossRef]
16. Davies, W.G.; Babamohammadi, S.; Yan, Y.; Clough, P.T.; Masoudi Soltani, S. Exergy analysis in intensification of sorption-enhanced steam methane reforming for clean hydrogen production: Comparative study and efficiency optimisation. *Carbon Capt. Sci. Technol.* **2024**, *12*, 100202. [CrossRef]
17. Wang, W.; Wang, S.; Ma, X.; Gong, J. Recent advances in catalytic hydrogenation of carbon dioxide. *Chem. Soc. Rev.* **2011**, *40*, 3703–3727. [CrossRef]
18. Centi, G.; Quadrelli, E.A.; Perathoner, S. Catalysis for CO_2 conversion: A key technology for rapid introduction of renewable energy in the value chain of chemical industries. *Energy Environ. Sci.* **2013**, *6*, 1711. [CrossRef]
19. Zhang, C.; Li, Y.; Chu, Z.; Fang, Y.; Han, K.; He, Z. Analysis of integrated CO_2 capture and utilization via calcium-looping in-situ dry reforming of methane and fischer-tropsch for synthetic fuels production. *Sep. Purif. Technol.* **2024**, *329*, 125109. [CrossRef]
20. Zhang, Z.; Huang, G.; Tang, X.; Yin, H.; Kang, J.; Zhang, Q.; Wang, Y. Zn and na promoted fe catalysts for sustainable production of high-valued olefins by CO_2 hydrogenation. *Fuel* **2022**, *309*, 122105. [CrossRef]
21. Wang, Y.; Gao, W.; Kazumi, S.; Fang, Y.; Shi, L.; Yoneyama, Y.; Yang, G.; Tsubaki, N. Solvent-free anchoring nano-sized zeolite on layered double hydroxide for highly selective transformation of syngas to gasoline-range hydrocarbons. *Fuel* **2019**, *253*, 249–256. [CrossRef]
22. Yang, L.; Pastor-Pérez, L.; Gu, S.; Sepúlveda-Escribano, A.; Reina, T.R. Highly efficient Ni/CeO_2-Al_2O_3 catalysts for CO_2 upgrading via reverse water-gas shift: Effect of selected transition metal promoters. *Appl. Catal. B Environ.* **2018**, *232*, 464–471. [CrossRef]
23. Galhardo, T.S.; Braga, A.H.; Arpini, B.H.; Szanyi, J.; Goncalves, R.V.; Zornio, B.F.; Miranda, C.R.; Rossi, L.M. Optimizing active sites for high co selectivity during CO_2 hydrogenation over supported nickel catalysts. *J. Am. Chem. Soc.* **2021**, *143*, 4268–4280. [CrossRef] [PubMed]
24. Lu, B.; Zhang, Z.; Li, X.; Luo, C.; Xu, Y.; Zhang, L. High-efficiency CuCe(rod) catalysts for CO_2 hydrogenation with high Cu content. *Fuel* **2020**, *276*, 118135. [CrossRef]
25. Chen, C.; Cheng, W.; Lin, S. Mechanism of CO formation in reverse water–gas shift reaction over Cu/Al_2O_3 catalyst. *Catal. Lett.* **2000**, *68*, 45–48. [CrossRef]
26. Chen, C.-S.; Cheng, W.-H.; Lin, S.-S. Study of iron-promoted Cu/SiO_2 catalyst on high temperature reverse water gas shift reaction. *Appl. Catal. A Gen.* **2004**, *257*, 97–106. [CrossRef]
27. Chen, C.S.; Cheng, W.H.; Lin, S.S. Study of reverse water gas shift reaction by TPD, TPR and CO_2 hydrogenation over potassium-promoted Cu/Sio_2 catalyst. *Appl. Catal. A Gen.* **2003**, *238*, 55–67. [CrossRef]
28. Jiang, X.; Nie, X.; Guo, X.; Song, C.; Chen, J.G. Recent advances in carbon dioxide hydrogenation to methanol via heterogeneous catalysis. *Chem. Rev.* **2020**, *120*, 7984–8034. [CrossRef]
29. Chen, A.; Yu, X.; Zhou, Y.; Miao, S.; Li, Y.; Kuld, S.; Sehested, J.; Liu, J.; Aoki, T.; Hong, S.; et al. Structure of the catalytically active copper–ceria interfacial perimeter. *Nat. Catal.* **2019**, *2*, 334–341. [CrossRef]
30. Konsolakis, M. The role of copper–ceria interactions in catalysis science: Recent theoretical and experimental advances. *Appl. Catal. B Environ.* **2016**, *198*, 49–66. [CrossRef]
31. Lu, B.; Xu, Y.; Zhang, Z.; Wu, F.; Li, X.; Luo, C.; Zhang, L. CO_2 hydrogenation on CeO_2@Cu catalyst synthesized via a solution auto-combustion method. *J. CO_2 Util.* **2021**, *54*, 101757. [CrossRef]
32. Muravev, V.; Spezzati, G.; Su, Y.-Q.; Parastaev, A.; Chiang, F.-K.; Longo, A.; Escudero, C.; Kosinov, N.; Hensen, E.J.M. Interface dynamics of Pd–CeO_2 single-atom catalysts during co oxidation. *Nat. Catal.* **2021**, *4*, 469–478. [CrossRef]
33. Dong, L.; Yao, X.; Chen, Y. Interactions among supported copper-based catalyst components and their effects on performance: A review. *Chin. J. Catal.* **2013**, *34*, 851–864. [CrossRef]
34. Zhou, G.; Dai, B.; Xie, H.; Zhang, G.; Xiong, K.; Zheng, X. Cecu composite catalyst for co synthesis by reverse water–gas shift reaction: Effect of Ce/Cu mole ratio. *J. CO_2 Util.* **2017**, *21*, 292–301. [CrossRef]
35. Lin, L.; Yao, S.; Liu, Z.; Zhang, F.; Li, N.; Vovchok, D.; Martínez-Arias, A.; Castañeda, R.; Lin, J.; Senanayake, S.D.; et al. In situ characterization of Cu/CeO_2 nanocatalysts for CO_2 hydrogenation: Morphological effects of nanostructured ceria on the catalytic activity. *J. Phys. Chem. C* **2018**, *122*, 12934–12943. [CrossRef]

36. Lu, B.; Zhang, T.; Zhang, L.; Xu, Y.; Zhang, Z.; Wu, F.; Li, X.; Luo, C. Promotion effects of oxygen vacancies on activity of na-doped CeO_2 catalysts for reverse water gas shift reaction. *Appl. Surf. Sci.* **2022**, *587*, 152881. [CrossRef]
37. Liu, Y.; Li, Z.; Xu, H.; Han, Y. Reverse water–gas shift reaction over ceria nanocube synthesized by hydrothermal method. *Catal. Commun.* **2016**, *76*, 1–6. [CrossRef]
38. Wang, W.; Zhang, Y.; Wang, Z.; Yan, J.; Ge, Q.; Liu, C. Reverse water gas shift over In_2O_3–CeO_2 catalysts. *Catal. Today* **2016**, *259*, 402–408. [CrossRef]
39. Zhou, Y.; Chen, A.; Ning, J.; Shen, W. Electronic and geometric structure of the copper-ceria interface on Cu/CeO_2 catalysts. *Chin. J. Catal.* **2020**, *41*, 928–937. [CrossRef]
40. Lu, B.; Wu, F.; Li, X.; Luo, C.; Zhang, L. Reconstruction of interface oxygen vacancy for boosting CO_2 hydrogenation by Cu/CeO_2 catalysts with thermal treatment. *Carbon Capt. Sci. Technol.* **2024**, *10*, 100173. [CrossRef]
41. Li, W.; Feng, X.; Zhang, Z.; Jin, X.; Liu, D.; Zhang, Y. A controllable surface etching strategy for well-defined spiny yolk@shell CuO@CeO_2 cubes and their catalytic performance boost. *Adv. Funct. Mater.* **2018**, *28*, 1802559. [CrossRef]
42. Cao, F.; Xiao, Y.; Zhang, Z.; Li, J.; Xia, Z.; Hu, X.; Ma, Y.; Qu, Y. Influence of oxygen vacancies of CeO_2 on reverse water gas shift reaction. *J. Catal.* **2022**, *414*, 25–32. [CrossRef]